

CERN-PH-EP-2020-ver.5.0
April 30, 2021

Probing transversity by measuring Λ polarisation in SIDIS

The COMPASS Collaboration

Abstract

Based on the observation of sizeable target-transverse-spin asymmetries in single-hadron and hadron-pair production in Semi-Inclusive measurements of Deep Inelastic Scattering (SIDIS), the chiral-odd transversity quark distribution functions h_1^q are nowadays well established. Several possible channels to access these functions were originally proposed. One candidate is the measurement of the polarisation of Λ hyperons produced in SIDIS off transversely polarised nucleons, where the transverse polarisation of the struck quark might be transferred to the final-state hyperon. In this article, we present the COMPASS results on the transversity-induced polarisation of Λ and $\bar{\Lambda}$ hyperons produced in SIDIS off transversely polarised protons. Within the experimental uncertainties, no significant deviation from zero was observed. The results are discussed in the context of different models taking into account previous experimental results on h_1^u and h_1^d .

(to be submitted to Physics Letters B)

The COMPASS Collaboration

G.D. Alexeev⁷, M.G. Alexeev^{26,27}, A. Amoroso^{26,27}, V. Andrieux^{9,28}, V. Anosov⁷, K. Augsten^{7,18}, W. Augustyniak²⁹, C.D.R. Azevedo¹, B. Badełek³⁰, F. Balestra^{26,27}, M. Ball³, J. Barth³, R. Beck³, Y. Bedfer²⁰, J. Berenguer Antequera^{26,27}, J. Bernhard^{12,9}, M. Bodlak¹⁷, F. Bradamante²⁵, A. Bressan^{24,25}, V.E. Burtsev²³, W.-C. Chang²¹, C. Chatterjee^{24,25}, M. Chiosso^{26,27}, A.G. Chumakov²³, S.-U. Chung^{15,a,b}, A. Cicuttin^{25,c}, P.M.M. Correia¹, M.L. Crespo^{25,c}, D. D'Agostino^{24,25}, S. Dalla Torre²⁵, S.S. Dasgupta⁶, S. Dasgupta²⁵, I. Denisenko⁷, O.Yu. Denisov^{27,#}, S.V. Donskov¹⁹, N. Doshita³², Ch. Dreisbach¹⁵, W. Dünnweber^d, R.R. Dusaev²³, A. Efremov⁷, C. Elia^{24,25}, P.D. Eversheim³, P. Faccioli¹¹, M. Faessler^d, A. Ferrero²⁰, M. Finger¹⁷, M. Finger Jr.¹⁷, H. Fischer⁸, C. Franco¹¹, J.M. Friedrich¹⁵, V. Frolov^{7,9}, L.G. Garcia Ordóñez^{24,25}, F. Gautheron^{2,28}, O.P. Gavrichtchouk⁷, S. Gerassimov^{14,15}, J. Giarra¹², I. Gnesi^{26,27}, D. Giordano²⁶, M. Gorzelli^{8,e}, A. Grasso^{26,27}, A. Gridin⁷, M. Grosse Perdekamp²⁸, B. Grube¹⁵, A. Guskov⁷, D. von Harrach¹², R. Heitz²⁸, N. Horikawa^{16,f}, N. d'Hose²⁰, C.-Y. Hsieh^{21,g}, S. Huber¹⁵, S. Ishimoto^{32,h}, A. Ivanov⁷, T. Iwata³², M. Jandek¹⁸, V. Jary¹⁸, R. Joosten^{3,#}, E. Kabuß¹², D.-H. Kang¹², F. Kaspar¹⁵, A. Kerbizi^{24,25}, B. Ketzer³, G.V. Khaustov¹⁹, Yu.A. Khokhlov^{19,i}, Yu. Kisselev^{7,j}, F. Klein⁴, J.H. Koivuniemi^{2,28}, V.N. Kolosov¹⁹, I. Konorov^{14,15}, V.F. Konstantinov¹⁹, A.M. Kotzinian^{27,k}, O.M. Kouznetsov⁷, A. Koval²⁹, Z. Kral¹⁷, F. Krinner¹⁵, Y. Kulinich²⁸, F. Kunne²⁰, K. Kurek²⁹, R.P. Kurjata³¹, A. Kveton¹⁷, K. Lavickova¹⁸, S. Levorato^{25,9}, Y.-S. Lian^{21,l}, J. Lichtenstadt²², P.-J. Lin^{20,m}, R. Longo²⁸, V. E. Lyubovitskij^{23,n}, A. Maggiora²⁷, A. Magnon^o, N. Makins²⁸, N. Makke^{25,c}, G.K. Mallot^{9,8}, A. Maltsev⁷, S. A. Mamon²³, B. Marianski^{29,j}, A. Martin^{24,25}, J. Marzec³¹, J. Matoušek^{17,25}, T. Matsuda¹³, G. Mattson²⁸, G.V. Meshcheryakov⁷, M. Meyer^{28,20}, W. Meyer², Yu.V. Mikhailov¹⁹, M. Mikhaylenko^{3,9}, E. Mitrofanov⁷, Y. Miyachi³², A. Moretti^{24,25,#}, A. Nagaytsev⁷, C. Naim²⁰, T.S. Negrini³, D. Neyret²⁰, J. Nový¹⁸, W.-D. Nowak¹², G. Nukazuka³², A.S. Nunes^{11,p}, A.G. Olshevsky⁷, M. Ostrick¹², D. Panzieri^{27,q}, B. Parsamyan^{26,27}, S. Paul¹⁵, H. Pekeler³, J.-C. Peng²⁸, M. Pešek¹⁷, D.V. Peshekhonov⁷, M. Pešková¹⁷, N. Pierre^{12,20}, S. Platchkov²⁰, J. Pochodzalla¹², V.A. Polyakov¹⁹, J. Pretz^{4,r}, M. Quaresima^{21,11}, C. Quintans¹¹, G. Reicherz², C. Riedl²⁸, T. Rudnicki³⁰, D.I. Ryabchikov^{19,15}, A. Rymbekova⁷, A. Rychter³¹, V.D. Samoylenko¹⁹, A. Sandacz²⁹, S. Sarkar⁶, I.A. Savin⁷, G. Sbrizzai^{24,25}, P. Schiavon^{24,25}, H. Schmieden⁴, A. Selyunin⁷, K. Sharkeev²³, L. Sinha⁶, M. Slunecka¹⁷, J. Smolik⁷, F. Sozzi²⁵, A. Srnka⁵, D. Steffen^{9,15}, M. Stolarski¹¹, O. Subrt^{9,18}, M. Sulc¹⁰, H. Suzuki^{32,f}, P. Sznajder²⁹, S. Tessaro²⁵, F. Tessarotto^{25,9,#}, A. Thiel³, J. Tomsa¹⁷, F. Tosello²⁷, A. Townsend²⁸, V. Tskhay¹⁴, S. Uhl¹⁵, A. Vauth^{4,9,s}, B. M. Veit^{12,9}, J. Veloso¹, B. Ventura²⁰, A. Vidon²⁰, M. Virius¹⁸, M. Wagner³, S. Wallner¹⁵, K. Zaremba³¹, P. Zavada⁷, M. Zavrtyaev¹⁴, M. Zemko^{18,9}, E. Zemlyanichkina⁷, Y. Zhao²⁵ and M. Ziembicki³¹

¹ University of Aveiro, I3N, Dept. of Physics, 3810-193 Aveiro, Portugal

² Universität Bochum, Institut für Experimentalphysik, 44780 Bochum, Germany^{t,u}

³ Universität Bonn, Helmholtz-Institut für Strahlen- und Kernphysik, 53115 Bonn, Germany^t

⁴ Universität Bonn, Physikalisches Institut, 53115 Bonn, Germany^t

⁵ Institute of Scientific Instruments of the CAS, 61264 Brno, Czech Republic^v

⁶ Matrivani Institute of Experimental Research & Education, Calcutta-700 030, India^w

⁷ Joint Institute for Nuclear Research, 141980 Dubna, Moscow region, Russia^x

⁸ Universität Freiburg, Physikalisches Institut, 79104 Freiburg, Germany^{t,u}

⁹ CERN, 1211 Geneva 23, Switzerland

¹⁰ Technical University in Liberec, 46117 Liberec, Czech Republic^v

¹¹ LIP, 1649-003 Lisbon, Portugal^y

¹² Universität Mainz, Institut für Kernphysik, 55099 Mainz, Germany^t

¹³ University of Miyazaki, Miyazaki 889-2192, Japan^z

¹⁴ Lebedev Physical Institute, 119991 Moscow, Russia

¹⁵ Technische Universität München, Physik Dept., 85748 Garching, Germany^{t,d}

- ¹⁶ Nagoya University, 464 Nagoya, Japan^z
- ¹⁷ Charles University, Faculty of Mathematics and Physics, 18000 Prague, Czech Republic^v
- ¹⁸ Czech Technical University in Prague, 16636 Prague, Czech Republic^v
- ¹⁹ State Scientific Center Institute for High Energy Physics of National Research Center ‘Kurchatov Institute’, 142281 Protvino, Russia
- ²⁰ IRFU, CEA, Université Paris-Saclay, 91191 Gif-sur-Yvette, France^u
- ²¹ Academia Sinica, Institute of Physics, Taipei 11529, Taiwan^{aa}
- ²² Tel Aviv University, School of Physics and Astronomy, 69978 Tel Aviv, Israel^{ab}
- ²³ Tomsk Polytechnic University, 634050 Tomsk, Russia^{ac}
- ²⁴ University of Trieste, Dept. of Physics, 34127 Trieste, Italy
- ²⁵ Trieste Section of INFN, 34127 Trieste, Italy
- ²⁶ University of Turin, Dept. of Physics, 10125 Turin, Italy
- ²⁷ Torino Section of INFN, 10125 Turin, Italy
- ²⁸ University of Illinois at Urbana-Champaign, Dept. of Physics, Urbana, IL 61801-3080, USA^{ad}
- ²⁹ National Centre for Nuclear Research, 02-093 Warsaw, Poland^{ae}
- ³⁰ University of Warsaw, Faculty of Physics, 02-093 Warsaw, Poland^{ae}
- ³¹ Warsaw University of Technology, Institute of Radioelectronics, 00-665 Warsaw, Poland^{ae}
- ³² Yamagata University, Yamagata 992-8510, Japan^z

Corresponding authors

E-mail addresses: Oleg.Denisov@cern.ch, Fulvio.Tessarotto@cern.ch

- ^a Also at Dept. of Physics, Pusan National University, Busan 609-735, Republic of Korea
- ^b Also at Physics Dept., Brookhaven National Laboratory, Upton, NY 11973, USA
- ^c Also at Abdus Salam ICTP, 34151 Trieste, Italy
- ^d Supported by the DFG cluster of excellence ‘Origin and Structure of the Universe’ (www.universe-cluster.de) (Germany)
- ^e Supported by the DFG Research Training Group Programmes 1102 and 2044 (Germany)
- ^f Also at Chubu University, Kasugai, Aichi 487-8501, Japan
- ^g Also at Dept. of Physics, National Central University, 300 Jhongda Road, Jhongli 32001, Taiwan
- ^h Also at KEK, 1-1 Oho, Tsukuba, Ibaraki 305-0801, Japan
- ⁱ Also at Moscow Institute of Physics and Technology, Moscow Region, 141700, Russia
- ^j Deceased
- ^k Also at Yerevan Physics Institute, Alikhanian Br. Street, Yerevan, Armenia, 0036
- ^l Also at Dept. of Physics, National Kaohsiung Normal University, Kaohsiung County 824, Taiwan
- ^m Supported by ANR, France with P2IO LabEx (ANR-10-LBX-0038) in the framework “Investissements d’Avenir” (ANR-11-IDEX-003-01)
- ⁿ Also at Institut für Theoretische Physik, Universität Tübingen, 72076 Tübingen, Germany
- ^o Retired
- ^p Present address: Brookhaven National Laboratory, Brookhaven, USA
- ^q Also at University of Eastern Piedmont, 15100 Alessandria, Italy
- ^r Present address: RWTH Aachen University, III. Physikalisches Institut, 52056 Aachen, Germany
- ^s Present address: Universität Hamburg, 20146 Hamburg, Germany
- ^t Supported by BMBF - Bundesministerium für Bildung und Forschung (Germany)
- ^u Supported by FP7, HadronPhysics3, Grant 283286 (European Union)
- ^v Supported by MEYS, Grant LM20150581 (Czech Republic)
- ^w Supported by B. Sen fund (India)
- ^x Supported by CERN-RFBR Grant 12-02-91500
- ^y Supported by FCT, Grants CERN/FIS-PAR/0007/2017 and CERN/FIS-PAR/0022/2019 (Portugal)
- ^z Supported by MEXT and JSPS, Grants 18002006, 20540299, 18540281 and 26247032, the Daiko and Yamada Foundations (Japan)

^{aa} Supported by the Ministry of Science and Technology (Taiwan)

^{ab} Supported by the Israel Academy of Sciences and Humanities (Israel)

^{ac} Supported by the Tomsk Polytechnic University within the assignment of the Ministry of Science and Higher Education (Russia)

^{ad} Supported by the National Science Foundation, Grant no. PHY-1506416 (USA)

^{ae} Supported by NCN, Grant 2017/26/M/ST2/00498 (Poland)

1 Introduction

The chiral-odd transversity quark distribution functions $h_1^q(x)$, hereafter referred to as transversity, were introduced as independent Parton Distribution Functions (PDFs) of the nucleon several decades ago [1–4]. Here, the superscript q denotes the quark flavour and x is the Bjorken variable. Several experimental approaches were proposed to access transversity in Semi-Inclusive measurements of Deep Inelastic Scattering (SIDIS) off transversely polarised nucleons.

Two of these approaches, the measurements of Collins asymmetries [5–8] and of azimuthal asymmetries of hadron pairs produced on transversely polarised protons [9–11], provided convincing evidence that transversity is indeed accessible experimentally. For u - and d -quarks, transversity was found to be different from zero at large x , where $h_1^u(x)$ and $h_1^d(x)$ are almost of the same size but opposite in sign, while $h_1^{\bar{u}}$ and $h_1^{\bar{d}}$ were found compatible with zero (see, e.g., Ref. [12]). However, the uncertainties for the $d(\bar{d})$ -quark are about a factor of 3(2) larger than the uncertainties for the $u(\bar{u})$ -quark, due to the unbalance of the existing proton and deuteron data.

A third approach, independent from the previous two, is the SIDIS measurement of the polarisation of baryons produced in the process $\ell p^\uparrow \rightarrow \ell B^\uparrow X$, where ℓ denotes a lepton, p^\uparrow a transversely polarised target proton and B a baryon [2, 13–15]. In the one-photon-exchange approximation, the hard interaction is $\gamma^* q^\uparrow \rightarrow q'^\uparrow$. When the virtual photon γ^* interacts with a transversely polarised quark q , the struck quark q' has a certain probability to transfer a fraction of the initial transverse polarisation to the final-state baryon. Thus a measurement of the polarisation of the final-state baryon along the spin direction of the outgoing quark allows access to transversity [16, 17].

Among all baryons, $\Lambda(\bar{\Lambda})$ hyperons are most suited to polarimetry studies due to their self-analysing weak decay into charged hadrons, $\Lambda \rightarrow p\pi^-$ ($\bar{\Lambda} \rightarrow \bar{p}\pi^+$), which occurs with a branching ratio $BR = 63.9\%$. The polarisation $P_{\Lambda(\bar{\Lambda})}$ is accessible through the modulation of the angular distribution of the decay protons (antiprotons):

$$\frac{dN_{p(\bar{p})}}{d\cos\theta} \propto 1 + \alpha_{\Lambda(\bar{\Lambda})} P_{\Lambda(\bar{\Lambda})} \cos\theta \quad , \quad (1)$$

where θ is the proton (antiproton) emission angle with respect to the polarisation axis of the fragmenting quark in the $\Lambda(\bar{\Lambda})$ rest frame and $\alpha_{\Lambda(\bar{\Lambda})}$ is the weak decay constant. For the analysis presented in this paper, we use the most recent values of $\alpha_{\Lambda(\bar{\Lambda})}$ [18], i.e., $\alpha_\Lambda = 0.750 \pm 0.009$ and $\alpha_{\bar{\Lambda}} = -0.758 \pm 0.010$.

As polarisation axis to access transversity we use the same that was used in QED calculations [19] for γ^* absorption. Accordingly, the components of the quark spins in initial (S_T) and final (S'_T) state in the γ^* -nucleon system are connected by

$$S'_{T,x} = -D_{NN} S_{T,x} \quad \text{and} \quad S'_{T,y} = D_{NN} S_{T,y}, \quad (2)$$

where as z -axis the virtual-photon direction is taken and as y -axis the normal to the lepton scattering (xz) plane (see Fig. 1). The virtual-photon depolarisation factor $D_{NN}(y) = 2(1-y)/(1+(1-y)^2)$ depends on y , the fraction of the initial lepton energy carried by the virtual photon in the target rest frame. The polarisation direction S'_T of the fragmenting quark is obtained as the reflection of the initial quark polarisation S_T with respect to the y -axis. As this direction is uncorrelated with the normal to the Λ production plane, no contribution of the spontaneous polarisation [20] is expected after integration over the azimuthal angle of this plane. Note that this is independent of the polarisation reversal described in Sec. 3. For the same reason, also the twist-3 terms related to the beam polarisation, which could contribute to the observed Λ polarisation along the S'_T direction (see e.g. Eqs. 100-102 in Ref. [21]), are expected to average to zero.

In the collinear approximation, where the intrinsic transverse momentum of the struck quark is assumed

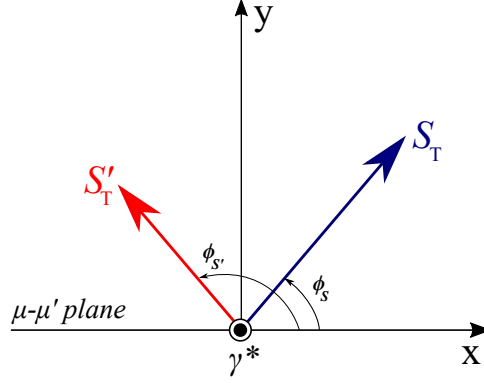


Fig. 1: Definition of the reference axes: The initial (S_T) and final (S'_T) transverse quark spin-polarisation vectors are shown with respect to the $\mu - \mu'$ scattering plane.

to be negligible, and in the current fragmentation region the expression for the transversity-induced $\Lambda(\bar{\Lambda})$ polarisation integrated over the hadron transverse momentum p_T reads [16]:

$$\begin{aligned}
 P_{\Lambda(\bar{\Lambda})}(x, z, Q^2) &= \frac{d\sigma^{\ell p^\dagger \rightarrow \ell' \Lambda(\bar{\Lambda})^\dagger X} - d\sigma^{\ell p^\dagger \rightarrow \ell' \Lambda(\bar{\Lambda})^\downarrow X}}{d\sigma^{\ell p^\dagger \rightarrow \ell' \Lambda(\bar{\Lambda})^\dagger X} + d\sigma^{\ell p^\dagger \rightarrow \ell' \Lambda(\bar{\Lambda})^\downarrow X}} \\
 &= f P_T D_{NN}(y) \frac{\sum_q e_q^2 h_1^q(x, Q^2) H_{1,q}^{\Lambda(\bar{\Lambda})}(z, Q^2)}{\sum_q e_q^2 f_1^q(x, Q^2) D_{1,q}^{\Lambda(\bar{\Lambda})}(z, Q^2)}.
 \end{aligned} \tag{3}$$

Here, Q^2 is the photon virtuality and z the fraction of the virtual photon energy carried by the $\Lambda(\bar{\Lambda})$ hyperon in the target rest frame; P_T is the target polarisation and f the target dilution factor representing the fraction of nucleons effectively polarised in the target. The sums in Eq.(3) run over all quark and antiquark flavours. The transversity distribution functions $h_1^q(x, Q^2)$ appear coupled to the chiral-odd fragmentation functions $H_{1,q}^{\Lambda(\bar{\Lambda})}(z, Q^2)$ that describe the spin transfer from the struck quark to the $\Lambda(\bar{\Lambda})$ hyperon:

$$H_{1,q}^{\Lambda(\bar{\Lambda})}(z, Q^2) = D_{1,q^\dagger}^{\Lambda(\bar{\Lambda})^\dagger}(z, Q^2) - D_{1,q^\dagger}^{\Lambda(\bar{\Lambda})^\downarrow}(z, Q^2). \tag{4}$$

The up and down arrows indicate the polarisation directions for the $\Lambda(\bar{\Lambda})$ along the S'_T axis. The polarisation-independent fragmentation functions $D_{1,q}^{\Lambda(\bar{\Lambda})}(z, Q^2)$ are given by

$$D_{1,q}^{\Lambda(\bar{\Lambda})}(z, Q^2) = D_{1,q^\dagger}^{\Lambda(\bar{\Lambda})^\dagger}(z, Q^2) + D_{1,q^\dagger}^{\Lambda(\bar{\Lambda})^\downarrow}(z, Q^2). \tag{5}$$

Evidently, this approach gives access to transversity only if at least a part of the quark spin is transferred to the final state hadron, i.e. if $H_{1,q}^{\Lambda(\bar{\Lambda})}(z, Q^2) \neq 0$. Alternatively, once transversity is known, $P_{\Lambda(\bar{\Lambda})}$ can be used to shed light on the size of the transverse-spin-dependent quark fragmentation function.

In general, $P_{\Lambda(\bar{\Lambda})}$ is not directly accessible from experimental data, as the detector acceptance distorts the angular distributions. Therefore, the measured angular distributions become

$$\frac{dN_{p(\bar{p})}}{d \cos \theta} \propto \left(1 + \alpha_{\Lambda(\bar{\Lambda})} P_{\Lambda(\bar{\Lambda})} \cos \theta\right) \cdot A(\theta), \tag{6}$$

where $A(\theta)$ is the detector acceptance depending on θ , which generally would have to be studied via detailed Monte Carlo simulations. However, in the COMPASS experiment [22] the specific target setup

offers the unique opportunity to measure the transversity-induced polarisation avoiding acceptance corrections (see Sec. 3).

The analysis presented here was performed using the data collected by COMPASS in 2007 and 2010 with a 160 GeV/c longitudinally polarised muon beam from the CERN SPS and a transversely polarised NH_3 target with proton polarisation $\langle P_T \rangle = 0.80$ and dilution factor $\langle f \rangle = 0.15$. In an earlier analysis, the $\Lambda(\bar{\Lambda})$ polarisation from the 2002-2004 data with a transversely polarised deuteron target [25] was found to be compatible with zero, as expected from the cancellation of u and d quark transversity (see Sec. 4.3). This measurement, however, suffered from limitations in statistical power and in spectrometer acceptance and from the lack of particle identification for a part of the data set. In this respect, the upcoming 2021/2022 run using a transversely polarised deuteron target [26] will be of great importance in drawing more definite conclusions.

2 Data selection and available statistics

In the data analysis, events are selected if they have at least one primary vertex, defined as the intersection point of a beam track, the scattered muon track, and other possible outgoing tracks. The primary vertex is required to be inside a target cell. The target consists of three cylindrical cells with 4 cm diameter, a central one of 60 cm and two outer ones of 30 cm length, each separated by 5 cm. Consecutive cells are polarised in opposite directions, so that data with both spin directions are recorded at the same time [6]. The extrapolated beam track is required to traverse all three target cells to ensure equal muon flux through the full target. Events originating from deep inelastic scattering are selected by requiring $Q^2 > 1$ (GeV/c)². For the invariant mass of the final state produced in the interaction of virtual-photon and nucleon, $W > 5$ GeV/c² is required to avoid the region of exclusive resonance production. Furthermore the constraints $0.003 < x < 0.7$ and $0.1 < y < 0.9$ are applied. Here, the upper limit in x avoids a region of low statistics, and in y the limits avoid large radiative corrections and contamination from final-state pion decay (upper limit) and warrant a good determination of y (lower limit).

The Λ and $\bar{\Lambda}$ reconstruction is based on the detection of their decay products that originate from a decay vertex (V^0) downstream of the production vertex, which is not connected to the latter by charged tracks. Due to the long Λ lifetime, $\tau = (2.632 \pm 0.020) \cdot 10^{-10}$ s, both vertices can be well separated. Exactly two oppositely charged hadrons with momentum larger than 1 GeV/c are required to originate from the decay vertex; the reconstructed momentum vector for such a hadron pair is required to be aligned with the vector linking the production and the decay vertices within a collinearity angle $\theta_{\text{coll}} \leq 7$ mrad. In order to suppress background from photon conversion $\gamma \rightarrow e^+e^-$, the transverse momentum p_{\perp} of each hadron, calculated with respect to the line-of-flight of the hadron pair in its rest frame, has to be larger than 23 MeV/c.

Particle identification is performed using the RICH detector. In order to limit the ambiguity between $\Lambda(\bar{\Lambda})$ hyperons and K_s^0 mesons decaying into $\pi^+\pi^-$, it is necessary to ensure that the positive (negative) daughter particle is a proton (antiproton). However, a direct identification would drastically reduce the available statistics due to the high Cherenkov threshold for protons of about 20 GeV/c for the radiator gas used (C_4F_{10}). Therefore, assuming one charged track as negative (positive) pion, the corresponding positive (negative) track is considered to be a proton (anti-proton) unless it is identified as positive (negative) electron, pion or kaon. The particle identification procedure is the same as it was used in previous analyses [27]. It is based on the calculation of the maximum likelihood \mathcal{L} for four mass hypotheses (e , K , π , p) and for the background, given the number of collected Cherenkov photons. In order to attribute a mass hypothesis M to a particle, \mathcal{L}_M is requested to be the highest and its ratio to the background hypothesis to be larger than an optimised threshold. This approach is applied to particles with momentum up to 50 GeV/c, a value at which pion/kaon separation becomes difficult. Beyond this limit, the highest likelihood is required not to be the one associated to the pion or kaon mass hypothesis.

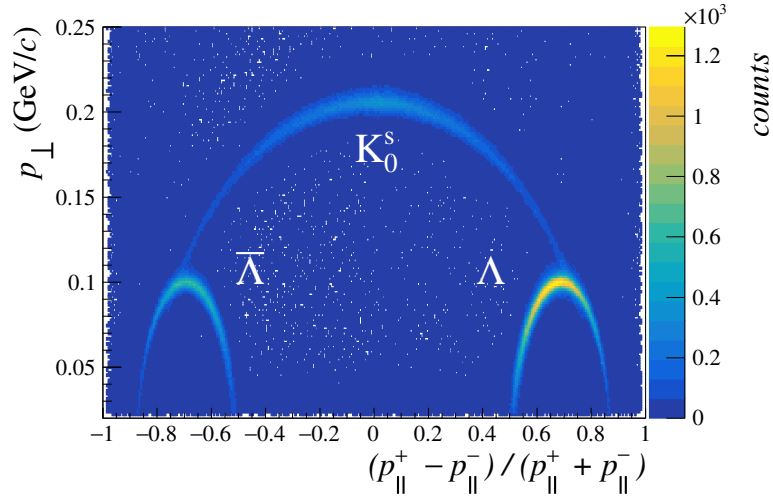


Fig. 2: Armenteros-Podolanski plot.

The Armenteros-Podolanski plot [28, 29] obtained after all aforementioned selection steps is shown in Fig. 2. The remaining K_s^0 contribution to the selected sample is visible as the symmetric arc, while a selection of the left and right halves of the figure allows to separate $\bar{\Lambda}$ (on the left) from Λ hyperons (on the right), based on the sign of the longitudinal momentum asymmetry $(p_{\parallel}^+ - p_{\parallel}^-)/(p_{\parallel}^+ + p_{\parallel}^-)$. Here, p_{\parallel}^+ (p_{\parallel}^-) indicates the longitudinal momentum of the positive (negative) decay particle in the hyperon rest frame with respect to the Λ ($\bar{\Lambda}$) line of flight. In Fig. 3 the Λ and $\bar{\Lambda}$ invariant mass spectra corresponding to these selections are shown. Here, only the K_s^0 in the crossing regions of the K_s^0 and Λ ($\bar{\Lambda}$) arcs contribute to the background. These invariant mass spectra are fitted with a superposition of a Gaussian function and a constant term using the PDG value for the Λ mass [30]. The background is evaluated with the sideband method considering two equally wide intervals on the left and on the right of the mass peak. Finally, hyperons are selected within a $\pm 3\sigma$ range from the peak, where $\sigma = 2.45 \text{ MeV}/c^2$ is obtained using all data shown in Fig. 3. Depending on the chosen kinematic bin, the signal-over-background ratio ranges from 5.7 to 54.9. The total statistics after background subtraction are given in Tab. 1.

A significant fraction of Λ and $\bar{\Lambda}$ particles originates from the decay of heavier hyperons. Using the

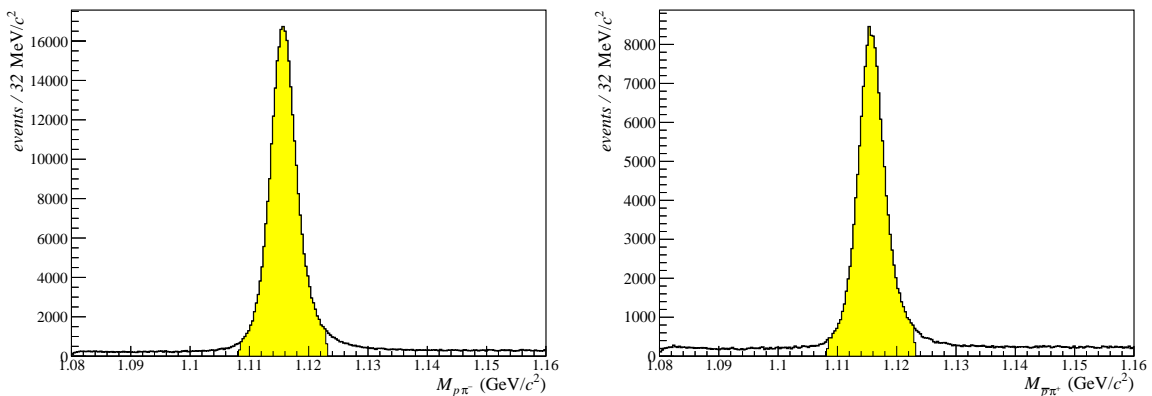


Fig. 3: Invariant mass spectra of Λ (left) and $\bar{\Lambda}$ (right) after all selection steps.

Table 1: Available statistics for Λ and $\bar{\Lambda}$ hyperons, after background subtraction, for years 2007 and 2010 and for their sum.

year	Λ	$\bar{\Lambda}$
2007	$95\,125 \pm 315$	$44\,911 \pm 227$
2010	$201\,421 \pm 466$	$99\,552 \pm 336$
total	$296\,546 \pm 562$	$144\,463 \pm 405$

event generator LEPTO based on the Lund string model [31], 63% of the Λ and 68% of the $\bar{\Lambda}$ hyperons produced in the COMPASS kinematic regime are estimated to originate from direct string fragmentation [32]. In this analysis, the Λ and $\bar{\Lambda}$ hyperons coming from indirect production cannot be separated from those coming from direct production. Their contribution is not taken into account as a systematic uncertainty in the analysis, although it could dilute a possible polarisation signal.

3 Extraction method and results for $\Lambda(\bar{\Lambda})$ polarisation

For this analysis, as for all target spin asymmetries measured at COMPASS, systematic effects are minimised due to the unique target configuration described at the beginning of the previous section and to the fact that the data taking is divided into periods, each consisting of two subperiods in which data are taken with reversed polarisation orientation in each target cell.

As the transversity-induced $\Lambda(\bar{\Lambda})$ polarisation is to be measured along the spin direction of the fragmenting quark, this reference axis has to be determined on an event-by-event basis. The initial-quark spin is assumed to be aligned with the nucleon spin and is thus vertical in the laboratory frame. Its transverse component is rotated by an azimuthal angle ϕ_S in the γ^* -nucleon system (Fig. 1). As described above, the spin direction of the quark after the interaction with the virtual photon is obtained by reflecting it with respect to the normal to the lepton scattering plane [17, 19, 23], $\phi_{S'} = \pi - \phi_S$. In the present analysis we determine the $\Lambda(\bar{\Lambda})$ polarisation along this direction.

The number of $\Lambda(\bar{\Lambda})$ hyperons emitting a proton (antiproton) in a given $\cos\theta$ range from a given target cell with a given direction of the target polarisation can be expressed as

$$\mathcal{N}_{\Lambda(\bar{\Lambda}),i}^{\{\prime\}}(\cos\theta) = \Phi_i^{\{\prime\}} \rho_i^{\{\prime\}} \bar{\sigma}_{\Lambda(\bar{\Lambda})} (1_{\{\pm\}} \alpha_{\Lambda(\bar{\Lambda})} P_{\Lambda(\bar{\Lambda})} \cos(\theta + (i-1)\pi)) A_i^{\{\prime\}}(\cos\theta). \quad (7)$$

Here, $i = 1, 2$ indicates the central or outer cells, respectively, $\Phi_i^{\{\prime\}}$ denotes the muon flux, $\rho_i^{\{\prime\}}$ the number of nucleons per unit area, and $\bar{\sigma}_{\Lambda(\bar{\Lambda})}$ is the cross section for the production of $\Lambda(\bar{\Lambda})$ hyperons. The acceptance term $A_i^{\{\prime\}}(\cos\theta)$ includes both geometrical acceptance, which is slightly different for each of the three target cells, and spectrometer efficiency. Primed quantities refer to data taken in subperiods after target polarisation reversal. After background subtraction, the four equations of Eq.(7) are combined to form a double ratio

$$\varepsilon_{\Lambda(\bar{\Lambda})}(\cos\theta) = \frac{\mathcal{N}_{\Lambda(\bar{\Lambda}),1}(\cos\theta) \mathcal{N}'_{\Lambda(\bar{\Lambda}),2}(\cos\theta)}{\mathcal{N}'_{\Lambda(\bar{\Lambda}),1}(\cos\theta) \mathcal{N}_{\Lambda(\bar{\Lambda}),2}(\cos\theta)}. \quad (8)$$

As described in Refs. [33, 34], the acceptances cancel in this expression as long as in each $\cos\theta$ bin the acceptance ratios for the target cells after polarisation reversal are equal to those before, which is a reasonable assumption for the given setup. As described above, equal muon flux in all three target cells is maintained by the event selection, so that also the flux cancels in Eq.(8). For small values of the $\Lambda(\bar{\Lambda})$ polarisation it then becomes:

$$\varepsilon_{\Lambda(\bar{\Lambda})}(\cos\theta) \approx 1 + 4\alpha_{\Lambda(\bar{\Lambda})} P_{\Lambda(\bar{\Lambda})} \cos\theta. \quad (9)$$

In each kinematic bin in x , z or p_T , the data sample is divided into eight $\cos\theta$ bins. This set of eight ε_j values is then fitted with the linear function $f = p_0(1 + p_1 \cos\theta)$, so that $P_{\Lambda(\bar{\Lambda})}$ is obtained as $P_{\Lambda(\bar{\Lambda})} = p_1/(4\alpha_{\Lambda(\bar{\Lambda})})$.

The transversity-induced polarisation is measured in the full phase-space and in the following regions:

- current fragmentation: $z \geq 0.2$ and Feynman variable $x_F > 0$;
- target fragmentation: $z < 0.2$ or $x_F < 0$;
- high x : $x \geq 0.032$;
- low x : $x < 0.032$;
- high p_T : $p_T \geq 0.5$ GeV/c;
- low p_T : $p_T < 0.5$ GeV/c.

In each of these regions, the data is scrutinised for possible systematic biases. The two main sources of systematic uncertainties are period compatibility and false $\Lambda(\bar{\Lambda})$ polarisations. The former are evaluated by comparing the results from the various periods of data taking, while the latter are evaluated by reshuffling the double ratio from Eq.(8) as $(\mathcal{N}_{\Lambda(\bar{\Lambda}),1} \mathcal{N}_{\Lambda(\bar{\Lambda}),2})/(\mathcal{N}'_{\Lambda(\bar{\Lambda}),1} \mathcal{N}'_{\Lambda(\bar{\Lambda}),2})$, so that transversity-induced $\Lambda(\bar{\Lambda})$ polarisations cancel. Effects of residual acceptance variations are proven to be negligible by evaluating the K_s^0 polarisation that is found to be compatible with zero as expected. In addition, $P_{\Lambda(\bar{\Lambda})}$ is measured assuming the central cell split into two halves, thus creating two data samples by combining each half with one of the outer cells. Again, effects of acceptance variation are found to be negligible. A scale uncertainty of about 7.5% contributes to the overall systematics due to the uncertainty on the weak decay constant α (2%) and on the dilution and polarisation factors f and P_T (5% overall). In general, $\sigma_{\text{syst}} < 0.85 \sigma_{\text{stat}}$. If the intrinsic transverse momentum k_T of the initial quark is not assumed to be zero, as it is done in the collinear approximation, the expression for P_Λ involves several other terms [35] dependent on the azimuthal angle ϕ of the $\Lambda(\bar{\Lambda})$ hyperon and on ϕ_S , which should be taken into consideration in case of a non-flat acceptance in terms of these angles. It was checked that the acceptance is flat over the azimuthal angle ϕ , so that after integration the contribution of ϕ -dependent terms vanishes. A remaining contribution of $\cos 2\phi_S$ -dependent terms can not a priori be excluded because the acceptance in ϕ_S is not flat. It was checked that the measured polarisations extracted for positive and negative values of $\cos 2\phi_S$ are consistent within statistical uncertainties, so that the contribution of $\cos 2\phi_S$ -dependent terms can be neglected.

In Fig. 4, the results from the full phase-space and for the current fragmentation region are presented in terms of the spin transfer

$$S_{\Lambda(\bar{\Lambda})} = \frac{P_{\Lambda(\bar{\Lambda})}}{f P_T D_{\text{NN}}(y)}, \quad (10)$$

by definition ranging from -1 to 1. The corresponding numerical values are given in the Appendix. The full set of data for all selections can be found on HEPDATA [36].

4 Interpretation of the results and predictions for future measurements

The polarisations shown in Fig. 4 are compatible with zero within the experimental uncertainties in all studied kinematic regions. From this result, applying different hypotheses, some conclusions will be drawn below on the size of the fragmentation function $H_{1,u}^\Lambda(z, Q^2)$ as well as on the strange quark

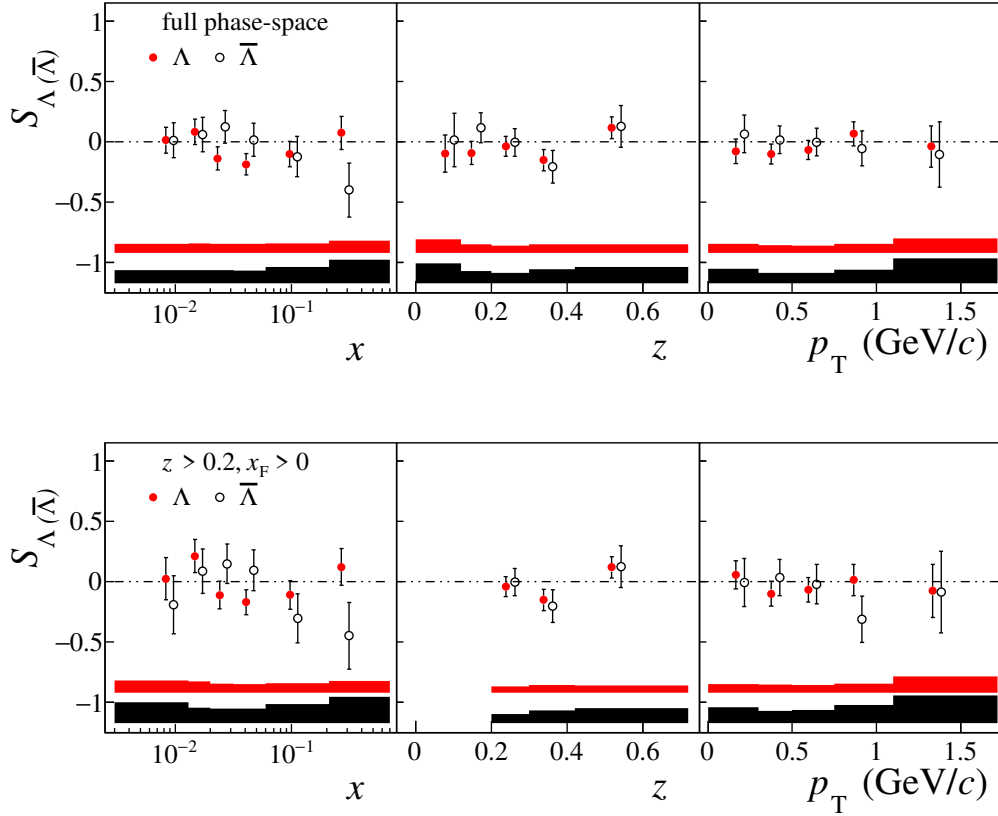


Fig. 4: Spin transfer $S_{\Lambda(\bar{\Lambda})}$ for the full phase-space (top) and for the current fragmentation region (bottom), as a function of x , z and p_T . The bands show the systematic uncertainties, while the error bars represent statistical uncertainties. The values in x , z and p_T are staggered for clarity.

transversity distribution $h_1^s(x, Q^2)$.

Following Eq.(3) and Eq.(10), in the current fragmentation region the spin transfer $S_{\Lambda(\bar{\Lambda})}$ reads

$$S_{\Lambda(\bar{\Lambda})} = \frac{\sum_q e_q^2 h_1^q H_{1,q}^{\Lambda(\bar{\Lambda})}}{\sum_q e_q^2 f_1^q D_{1,q}^{\Lambda(\bar{\Lambda})}}, \quad (11)$$

where the dependences on x , z and Q^2 are omitted for simplicity.

4.1 Interpretation of the measured $\bar{\Lambda}$ polarisation

Considering the case of $\bar{\Lambda}$ hyperons, the favoured fragmentation functions $H_{1,\bar{u}}^{\bar{\Lambda}}$, $H_{1,\bar{d}}^{\bar{\Lambda}}$ and $H_{1,\bar{s}}^{\bar{\Lambda}}$ only appear in combination with the sea-quarks \bar{u} , \bar{d} and \bar{s} . As $h_1^{\bar{s}} \approx 0$ can be assumed in analogy to $h_1^{\bar{u}}$ and $h_1^{\bar{d}}$, transversity is coupled only to unfavoured fragmentation functions. Here $H_{1,u}^{\bar{\Lambda}}$ and $H_{1,d}^{\bar{\Lambda}}$ dominate, as the s -quark contribution $h_1^s H_{1,s}^{\bar{\Lambda}}$ can be neglected because also h_1^s is expected to be small. This yields

$$\sum_q e_q^2 h_1^q H_{1,q}^{\bar{\Lambda}} \propto 4h_1^u H_{1,u}^{\bar{\Lambda}} + h_1^d H_{1,d}^{\bar{\Lambda}}. \quad (12)$$

The compatibility with zero of the measured polarisation for $\bar{\Lambda}$ hyperons is in agreement with expectations based on calculations for the ratios of favoured to unfavoured fragmentation functions (see, e.g., Ref. [37]). In these calculations, the unfavoured fragmentation functions are suppressed by a factor of about 4 to 5 in the current fragmentation region at z about 0.2 and rapidly decrease further for increasing z .

4.2 Interpretation of the measured Λ polarisation

Considering the case of Λ hyperons, one of the options suggested in e.g. Ref. [37] is to retain only the favoured combinations ($H_{1,u}^\Lambda$, $H_{1,d}^\Lambda$, $H_{1,s}^\Lambda$, $D_{1,u}^\Lambda$, $D_{1,d}^\Lambda$, $D_{1,s}^\Lambda$) in both numerator and denominator, resulting in:

$$S_\Lambda = \frac{4h_1^u H_{1,u}^\Lambda + h_1^d H_{1,d}^\Lambda + h_1^s H_{1,s}^\Lambda}{4f_1^u D_{1,u}^\Lambda + f_1^d D_{1,d}^\Lambda + f_1^s D_{1,s}^\Lambda}. \quad (13)$$

Isospin symmetry requires $D_{1,d}^\Lambda = D_{1,u}^\Lambda$ and $H_{1,d}^\Lambda = H_{1,u}^\Lambda$. For the s -quark fragmentation functions, it is often assumed that $D_{1,s}^\Lambda$ is proportional to $D_{1,u}^\Lambda$ with the proportionality constant r , which is the inverse of the strangeness suppression factor $\lambda = 1/r$ [38, 39]. In Ref. [40] its value is obtained from a fit of experimental baryon production data in e^+e^- annihilation to be $\lambda_\Lambda = 1/r = 0.44$. With these simplifications, Eq.(13) turns into

$$S_\Lambda = \frac{[4h_1^u + h_1^d] H_{1,u}^\Lambda + h_1^s H_{1,s}^\Lambda}{[4f_1^u + f_1^d + r f_1^s] D_{1,u}^\Lambda}. \quad (14)$$

The interpretation is now performed in three different scenarios. When needed, we use the CTEQ5D PDFs [41] for f_1^q , calculated at the x and Q^2 values of the data points, while the values of the transversity functions for u and d quarks are obtained from the fit presented in Ref. [12].

i) Transversity is non-zero only for valence quarks in the nucleon

If transversity is assumed non-vanishing only for valence quarks, h_1^s can be neglected and the expression for the spin transfer to the Λ further simplifies to:

$$S_\Lambda = \frac{[4h_1^u + h_1^d] H_{1,u}^\Lambda}{[4f_1^u + f_1^d + r f_1^s] D_{1,u}^\Lambda}. \quad (15)$$

When S_Λ is now inspected only as a function of x , its dependence upon z , carried by the fragmentation functions, is integrated over. In a generic x bin centered at x^* it becomes

$$S_\Lambda|_{x=x^*} = \frac{[4h_1^u(x^*) + h_1^d(x^*)] \int_{0.2}^{1.0} dz H_{1,u}^\Lambda(z)}{[4f_1^u(x^*) + f_1^d(x^*) + r f_1^s(x^*)] \int_{0.2}^{1.0} dz D_{1,u}^\Lambda(z)}. \quad (16)$$

Thus the measurement of S_Λ as a function of x can be used to extract, in each bin of x , the ratio \mathcal{R} of the z -integrated fragmentation functions $H_{1,u}^\Lambda$ and $D_{1,u}^\Lambda$:

$$\mathcal{R}(x^*) = \frac{\int_{0.2}^{1.0} dz H_{1,u}^\Lambda(z)}{\int_{0.2}^{1.0} dz D_{1,u}^\Lambda(z)} \Big|_{x=x^*} = \frac{4f_1^u(x^*) + f_1^d(x^*) + r f_1^s(x^*)}{4h_1^u(x^*) + h_1^d(x^*)} S_\Lambda|_{x=x^*}. \quad (17)$$

In Tab. 2 the mean values of \mathcal{R} over the measured x range are given for three different choices of r . These values, which show a weak dependence on r , are all negative and still compatible with zero within the given uncertainties.

Table 2: Mean value $\langle \mathcal{R} \rangle$ of the ratio of the z -integrated fragmentation functions for three choices of r . The uncertainties are statistical only.

r	$\langle \mathcal{R} \rangle \pm \sigma_{\langle \mathcal{R} \rangle}$
2	-0.27 ± 0.55
3	-0.27 ± 0.56
4	-0.26 ± 0.57

ii) Λ polarisation is carried by the s quark only

Assuming instead that the polarisation is entirely carried by the s quark, as in the SU(3) non-relativistic quark model, $H_{1,u}^\Lambda$ can be neglected. Moreover, as suggested by Ref. [42], $H_{1,s}^\Lambda$ can be approximated with $D_{1,s}^\Lambda$ for $z > 0.2$, yielding

$$S_\Lambda = \frac{h_1^s H_{1,s}^\Lambda}{[4f_1^u + f_1^d + r f_1^s] \frac{1}{r} D_{1,s}^\Lambda} \approx \frac{r h_1^s}{4f_1^u + f_1^d + r f_1^s}, \quad (18)$$

so that h_1^s can be extracted. In Fig. 5 the quantity $xh_1^s(x)$ is given for various choices of r and compared to the fitted value and accuracy of the $xh_1^u(x)$ distribution [12]. Again, only a weak dependence on r is observed. Although the data suggest a negative sign of $h_1^s(x)$, they are not precise enough to determine accurately $h_1^s(x)$ compared to the statistical precision of the $h_1^u(x)$ data.

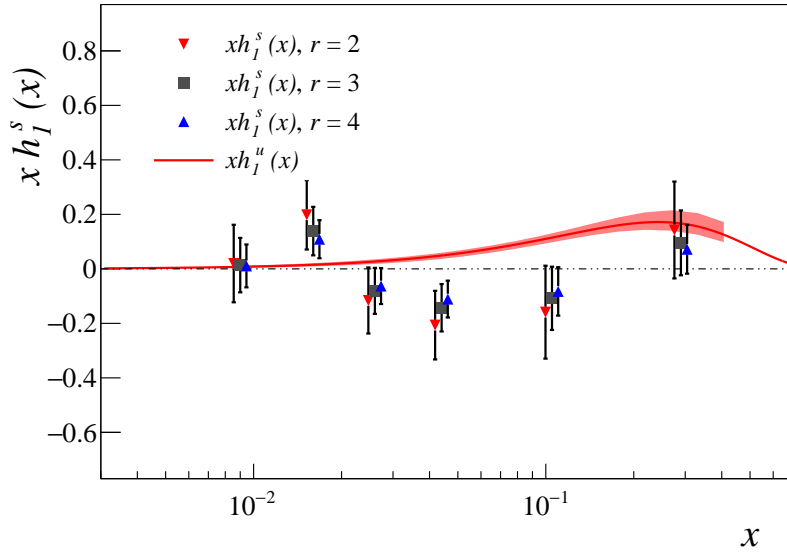


Fig. 5: Extracted values of $xh_1^s(x)$ for the three options $r = 2, 3, 4$. The u quark transversity curve from Ref. [12] is given for comparison. Only statistical uncertainties are shown and the x values are staggered for clarity.

iii) Polarised- Λ production is described by a quark-diquark fragmentation model

In the context of the quark-diquark model [42, 43], the fragmentation of an unpolarised valence quark q into a final-state hadron is accompanied by the emission of a diquark D , which can be in a scalar

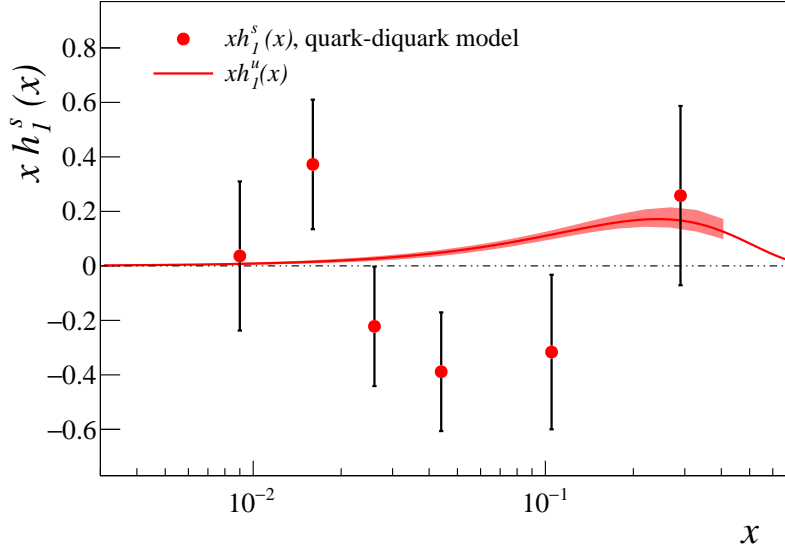


Fig. 6: Extracted values of $xh_1^s(x)$ according to a quark-diquark model [42, 43]. The u quark transversity curve from Ref. [12] is given for comparison. Only statistical uncertainties are shown.

(S) or vector (V) spin configuration. The probabilities $a_D^{(q)}(z)$ associated to these two configurations are calculated in the model and enter the definition of the quark fragmentation function, which depends on z and on the masses of the fragmenting quark, the diquark and the produced hadron. Analogously, the fragmentation of a polarised quark is described through the probabilities $\hat{a}_D^{(q)}(z)$. In the case of Λ production, the unpolarised fragmentation function of the s quark, $D_{1,s}^\Lambda$, is taken as reference and used to express all the other fragmentation functions by introducing the flavour structure ratios $F_S^{(u/s)}(z) = a_S^{(u)}(z)/a_S^{(s)}(z)$, $F_M^{(u/s)}(z) = a_V^{(u)}(z)/a_S^{(s)}(z)$ and the spin-structure ratios $\hat{W}_D^q(z) = \hat{a}_D^{(q)}(z)/a_D^{(q)}(z)$. The transversity-induced polarisation can thus be written as:

$$S_\Lambda = \frac{(4h_1^u + h_1^d) \cdot \frac{1}{4} [\hat{W}_S^{(u)} F_S^{(u/s)} - \hat{W}_V^{(u)} F_M^{(u/s)}] + h_1^s \hat{W}_S^{(s)}}{(4f_1^u + f_1^d) \cdot \frac{1}{4} [F_S^{(u/s)} + 3F_M^{(u/s)}] + f_1^s}, \quad (19)$$

where the x and z dependences are omitted for clarity. Information on h_1^s can be obtained by integrating Eq.(19) over z in each x bin. The values of $xh_1^s(x)$, as predicted by the quark-diquark model and based on the measured polarisation, are shown in Fig. 6. The dependence of the final results on the mass of the diquark (containing or not the s quark) was found negligible.

Again, as in scenario ii), the data suggest a negative sign of $h_1^s(x)$, but statistical uncertainties are even larger in this case. Improved data will be needed to determine $h_1^s(x)$ more accurately.

4.3 Projections for future data taking with transversely polarised deuterons

The upcoming COMPASS run aims at collecting new precision SIDIS data using a polarised deuteron (LiD) target. The expected statistical uncertainties of the measured asymmetries are in the order of 60% of those estimated for the proton data. Compared to the existing deuteron data taken with the early

COMPASS setup, we expect an accuracy improvement between a factor of two at small x and a factor of five at large x [26]. Some prospects for this measurement are described in the following.

The expression for the spin transfer, for Λ production on a transversely-polarised deuteron target, reads:

$$S_{\Lambda}^D = \frac{5(h_1^u + h_1^d)H_{1,u}^{\Lambda} + 2h_1^s H_{1,s}^{\Lambda}}{5(f_1^u + f_1^d)D_{1,u}^{\Lambda} + 2f_1^s D_{1,s}^{\Lambda}}. \quad (20)$$

It is already known from earlier COMPASS data that $h_1^d \approx -h_1^u$ [44, 45]. The upcoming COMPASS run on a deuteron target will, in addition, allow us to measure with high precision the quantity $h_1^u + h_1^d$. Since the fragmentation function $H_{1,u}^{\Lambda}$ is expected to be smaller than the fragmentation function $H_{1,s}^{\Lambda}$, the numerator of Eq.(20) will be dominated by the product $h_1^s H_{1,s}^{\Lambda}$ if h_1^s is of significant size. Therefore, a new high statistics measurement of the transversity-induced Λ polarisation on a deuteron target from the upcoming data is expected to be very sensitive to the product $h_1^s H_{1,s}^{\Lambda}$.

5 Summary and outlook

Using a transversely polarised proton target and a 160 GeV/ c muon beam, the transversity-induced polarisation along the spin axis of the struck quark was measured by COMPASS for Λ and $\bar{\Lambda}$ hyperons. While considered to be an excellent channel to access transversity, the results were found to be compatible with zero in all studied kinematic regions.

The statistical uncertainty on the measured polarisation is still large, despite the fact that all COMPASS data on a transversely polarised proton target were used, which are the only existing world data suitable for this measurement. Nevertheless, some information could be deduced from the existing data.

Under the hypothesis that transversity is non-vanishing only for valence quarks, the data were used to investigate the ratio of z -integrated polarised to unpolarised fragmentation functions. The results indicate a negative ratio, although compatible with zero due to the large uncertainties. If instead a non-relativistic SU(3) quark model or a quark-diquark model is considered, some information can be derived on the transversity distribution for the s quark. In both cases the results tend to support a negative s -quark transversity h_1^s within the large uncertainties given.

In addition, some prospects were given for measuring precisely the transversity-induced polarisation of Λ hyperons produced on a transversely polarised deuteron target. Since such a measurement is anticipated to be very sensitive to h_1^s , the results expected from the upcoming COMPASS run with a transversely polarised deuteron target in the years 2021 and 2022 will help to improve our knowledge on transversity.

Acknowledgements

We gratefully acknowledge the support of CERN management and staff and the skill and effort of the technicians of our collaborating institutions.

Appendix

Here, the spin transfer for Λ and $\bar{\Lambda}$ hyperons is given for the full phase-space and for the current fragmentation region. For each bin the kinematic range is indicated, together with the mean values of x , Q^2 , z and p_T . These and other tables, for all the aforementioned kinematic regions, are available on HEPDATA.

Table 3: Spin transfer $S_{\Lambda(\bar{\Lambda})}$ from the full phase-space, as a function of x , z and p_T . For each kinematic bin the mean values of x , Q^2 , z and p_T are also given.

Full phase space						
x range	$\langle x \rangle$	$\langle Q^2 \rangle$ (GeV/c) ²	$\langle z \rangle$	$\langle p_T \rangle$ (GeV/c)	S_Λ	$S_{\bar{\Lambda}}$
0.003 - 0.013	0.009	1.49	0.20	0.60	$0.014 \pm 0.106 \pm 0.074$	$0.014 \pm 0.145 \pm 0.107$
0.013 - 0.020	0.016	2.06	0.25	0.59	$0.083 \pm 0.104 \pm 0.078$	$0.061 \pm 0.141 \pm 0.108$
0.020 - 0.032	0.025	2.75	0.28	0.57	$-0.138 \pm 0.096 \pm 0.077$	$0.125 \pm 0.134 \pm 0.107$
0.032 - 0.060	0.044	4.30	0.31	0.55	$-0.186 \pm 0.089 \pm 0.076$	$0.017 \pm 0.138 \pm 0.102$
0.060 - 0.210	0.104	9.54	0.32	0.52	$-0.101 \pm 0.105 \pm 0.080$	$-0.122 \pm 0.169 \pm 0.132$
0.210 - 0.700	0.290	26.5	0.34	0.53	$0.074 \pm 0.138 \pm 0.101$	$-0.399 \pm 0.224 \pm 0.193$
z range	$\langle x \rangle$	$\langle Q^2 \rangle$ (GeV/c) ²	$\langle z \rangle$	$\langle p_T \rangle$ (GeV/c)	S_Λ	$S_{\bar{\Lambda}}$
0.00 - 0.12	0.023	4.15	0.09	0.55	$-0.097 \pm 0.154 \pm 0.114$	$0.015 \pm 0.222 \pm 0.163$
0.12 - 0.20	0.031	4.14	0.16	0.57	$-0.092 \pm 0.095 \pm 0.073$	$0.117 \pm 0.123 \pm 0.099$
0.20 - 0.30	0.041	4.13	0.25	0.57	$-0.038 \pm 0.083 \pm 0.060$	$-0.005 \pm 0.113 \pm 0.083$
0.30 - 0.42	0.050	4.11	0.35	0.56	$-0.152 \pm 0.087 \pm 0.072$	$-0.205 \pm 0.136 \pm 0.114$
0.42 - 1.00	0.058	3.99	0.53	0.58	$0.118 \pm 0.090 \pm 0.071$	$0.127 \pm 0.173 \pm 0.136$
p_T range (GeV/c)	$\langle x \rangle$	$\langle Q^2 \rangle$ (GeV/c) ²	$\langle z \rangle$	$\langle p_T \rangle$ (GeV/c)	S_Λ	$S_{\bar{\Lambda}}$
0.00 - 0.30	0.045	4.33	0.27	0.19	$-0.079 \pm 0.101 \pm 0.076$	$0.066 \pm 0.158 \pm 0.120$
0.30 - 0.50	0.042	4.20	0.26	0.40	$-0.101 \pm 0.082 \pm 0.064$	$0.016 \pm 0.114 \pm 0.085$
0.50 - 0.75	0.039	4.02	0.26	0.62	$-0.066 \pm 0.079 \pm 0.059$	$-0.002 \pm 0.115 \pm 0.084$
0.75 - 1.10	0.036	3.91	0.27	0.89	$0.068 \pm 0.099 \pm 0.074$	$-0.054 \pm 0.145 \pm 0.110$
1.10 - 3.50	0.034	3.97	0.28	1.35	$-0.039 \pm 0.172 \pm 0.122$	$-0.104 \pm 0.271 \pm 0.206$

Table 4: Spin transfer $S_{\Lambda(\bar{\Lambda})}$ from the current fragmentation region ($z \geq 0.2$, $x_F > 0$), as a function of x , z and p_T . For each kinematic bin the mean values of x , Q^2 , z and p_T are also given.

Current fragmentation region						
x range	$\langle x \rangle$	$\langle Q^2 \rangle$ (GeV/c) ²	$\langle z \rangle$	$\langle p_T \rangle$ (GeV/c)	S_Λ	$S_{\bar{\Lambda}}$
0.003 - 0.013	0.009	1.42	0.31	0.62	$0.024 \pm 0.174 \pm 0.104$	$-0.190 \pm 0.241 \pm 0.173$
0.013 - 0.020	0.016	1.81	0.33	0.60	$0.212 \pm 0.136 \pm 0.096$	$0.088 \pm 0.184 \pm 0.128$
0.020 - 0.032	0.026	2.31	0.35	0.57	$-0.110 \pm 0.115 \pm 0.075$	$0.148 \pm 0.164 \pm 0.119$
0.032 - 0.060	0.044	3.60	0.37	0.54	$-0.169 \pm 0.103 \pm 0.073$	$0.096 \pm 0.169 \pm 0.119$
0.060 - 0.210	0.105	8.19	0.38	0.51	$-0.110 \pm 0.118 \pm 0.077$	$-0.303 \pm 0.203 \pm 0.156$
0.210 - 0.700	0.290	23.4	0.38	0.53	$0.122 \pm 0.152 \pm 0.098$	$-0.448 \pm 0.276 \pm 0.215$
z range	$\langle x \rangle$	$\langle Q^2 \rangle$ (GeV/c) ²	$\langle z \rangle$	$\langle p_T \rangle$ (GeV/c)	S_Λ	$S_{\bar{\Lambda}}$
0.20 - 0.30	0.040	4.12	0.25	0.57	$-0.039 \pm 0.083 \pm 0.052$	$-0.003 \pm 0.113 \pm 0.074$
0.30 - 0.42	0.050	4.12	0.35	0.56	$-0.152 \pm 0.087 \pm 0.063$	$-0.202 \pm 0.136 \pm 0.104$
0.42 - 1.00	0.058	3.99	0.53	0.58	$0.119 \pm 0.090 \pm 0.062$	$0.126 \pm 0.173 \pm 0.123$
p_T range (GeV/c)	$\langle x \rangle$	$\langle Q^2 \rangle$ (GeV/c) ²	$\langle z \rangle$	$\langle p_T \rangle$ (GeV/c)	S_Λ	$S_{\bar{\Lambda}}$
0.00 - 0.30	0.052	4.24	0.35	0.19	$0.056 \pm 0.117 \pm 0.073$	$-0.007 \pm 0.199 \pm 0.131$
0.30 - 0.50	0.051	4.19	0.35	0.40	$-0.099 \pm 0.104 \pm 0.069$	$0.036 \pm 0.151 \pm 0.102$
0.50 - 0.75	0.047	4.01	0.35	0.62	$-0.068 \pm 0.102 \pm 0.065$	$-0.021 \pm 0.163 \pm 0.109$
0.75 - 1.10	0.043	3.89	0.36	0.89	$0.014 \pm 0.128 \pm 0.076$	$-0.310 \pm 0.191 \pm 0.149$
1.10 - 3.50	0.039	3.99	0.36	1.36	$-0.076 \pm 0.219 \pm 0.134$	$-0.086 \pm 0.338 \pm 0.229$

References

- [1] J.P. Ralston and D.E. Soper, Nucl. Phys. B 152 (1979) 109.
- [2] F. Baldracchini, N.S. Craigie, V. Roberto and M. Socolovsky, Fortsch. Phys. 30 (1981) 505.
- [3] X. Artru and M. Mekhfi, Z. Phys. C 45 (1990) 669.
- [4] R.L. Jaffe and X. Ji, Phys. Rev. Lett. 67 (1991) 552.
- [5] A. Airapetian, et al., HERMES Collaboration, Phys. Lett. B 693 (2010) 11.
- [6] M. G. Alekseev, et al., COMPASS Collaboration, Phys. Lett. B 692 (2010) 240.
- [7] C. Adolph, et al., COMPASS Collaboration, Phys. Lett. B 717 (2012) 376.
- [8] A. Airapetian, et al., HERMES Collaboration, Phys. Rev. Lett. 94 (2005) 012002.
- [9] A. Airapetian, et al., HERMES Collaboration, J. High Energy Phys. 06 (2008) 017.
- [10] C. Adolph, et al., COMPASS Collaboration, Phys. Lett. B 713 (2012) 10.
- [11] C. Adolph, et al., COMPASS Collaboration, Phys. Lett. B 736 (2014) 124.
- [12] A. Martin, F. Bradamante and V. Barone, Phys. Rev. D 91 (2015) 014034.
- [13] R.L. Jaffe, Phys. Rev. D 54 (1996) 11.
- [14] X. Artru and M. Mekhfi, Nucl. Phys. A 532 (1991) 351.

- [15] M. Anselmino, arXiv:hep-ph/0302008.
- [16] M. Anselmino, M. Boglione and F. Murgia, *Phys. Lett. B* 481 (2000) 253.
- [17] V. Barone and P.G. Ratcliffe, *Transverse spin physics*, World Scientific, River Edge, USA 2003.
- [18] M. Ablikim, et al., BESIII Collaboration, *Nature Phys.* 15 (2019) 631.
- [19] A. Kotzinian, *Nucl. Phys. B* 441 (1995) 234.
- [20] G. Bunce, et al., *Phys. Rev. Lett.* 36 (1976) 1113.
- [21] P.J. Mulders and R.D. Tangerman, *Nucl. Phys. B* 461 (1996) 197.
- [22] P. Abbon, et al., COMPASS Collaboration, *Nucl. Instrum. Meth. A* 577 (2007) 455.
- [23] G. Baum, et al., COMPASS Collaboration, COMPASS: A Proposal for a Common Muon and Proton Apparatus for Structure and Spectroscopy, CERN-SPSLC-96-14, CERN-SPSLC-P-297.
- [24] T. Negri, *AIP Conf. Proc.* 1149 (2009) 656.
- [25] A. Ferrero, *AIP Conf. Proc.* 915 (2007) 436.
- [26] K. Augsten, et al., COMPASS Collaboration and PNPI, Addendum to the COMPASS-II Proposal, CERN-SPSC-2017-034, SPSC-P-340-ADD-1.
- [27] P. Abbon, et al., *Nucl. Instrum. Meth. A* 631 (2011) 26.
- [28] J. Podolanski and R. Armenteros, *Lond. Edinb. Dubl. Phil. Mag.* 45 (1954) 13.
- [29] R. Armenteros, et al., *Lond. Edinb. Dubl. Phil. Mag.* 43 (1952) 597.
- [30] M. Tanabashi, et al., The Particle Data Group, *Phys. Rev. D* 98 (2018) 030001.
- [31] G. Ingelman, A. Edin and J. Rathsmann, *Comput. Phys. Commun.* 101 (1997) 108.
- [32] C. Adolph, et al., COMPASS Collaboration, *Eur. Phys. J. C* 73 (2013) 10.
- [33] V.Yu. Alexakhin, et al., COMPASS Collaboration, *Phys. Rev. Lett.* 94 (2005) 202002.
- [34] E. S. Ageev, et al., COMPASS Collaboration, *Nucl. Phys. B* 765 (2007) 31.
- [35] D. Boer, R. Jakob and P.J. Mulders, *Nucl. Phys. B* 564 (2000) 471.
- [36] E. Maguire, L. Heinrich and G. Watt, *J. Phys. Conf. Ser.* 898 (2017) 102006.
- [37] B.-Q. Ma, I. Schmidt and J.-J. Yang, *Phys. Lett. B* 574 (2003) 35.
- [38] D. Indumathi, H. S. Mani, and A. Rastogi, *Phys. Rev. D* 58 (1998) 094014.
- [39] A. Rastogi, *Phys. Rev. D* 59 (1999) 114012.
- [40] J.-J. Yang, *Phys. Rev. D* 65 (2002) 094035.
- [41] A. Buckley, et al., *Eur. Phys. J. C* 75 (2015) 132.
- [42] J.-J. Yang, *Nucl. Phys. A* 699 (2002) 562.
- [43] R. Jakob, P.J. Mulders and J. Rodrigues, *Nucl. Phys. A* 626 (1997) 937.
- [44] V. Barone, et al., *Phys. Rev. D* 99 (2019) 114004.
- [45] M. Anselmino, A. Mukherjee and A. Vossen, *Prog. Part. Nucl. Phys.* 114 (2020) 103806.